Avalanche correlations in the martensitic transition of a Cu-Zn-Al shape memory alloy: analysis of acoustic emission and calorimetry

Jordi Baró[1], José-María Martín-Olalla[2], Francisco Javier Romero[2], María Carmen Gallardo[2], Ekhard K.H.Salje[3], Eduard Vives[1] and Antoni Planes[1].

[1]Departament d'Estructura i Constituents de la Matèria. Facultat de Física. Universitat de Barcelona. Diagonal, 647, E-08028 Barcelona, Catalonia, Spain
[2]Departamento de Física de la Materia Condensada, Universidad de Sevilla, P.O. Box 1065, E-41080 Sevilla, Spain.
Department of Earth Sciences, University of Cambridge, Downing Street, Cambridge CB2 3EQ, United Kingdom.

Abstract. The existence of temporal correlations during the intermittent dynamics of a thermally driven structural phase transition is studied in a Cu-Zn-Al alloy. The sequence of avalanches is observed by means of two techniques: acoustic emission and high sensitivity calorimetry. Both methods reveal the existence of event clustering in a way that is equivalent to the Omori correlations between aftershocks in earth quakes as is commonly used in seismology.

PACS numbers: 81.30.Kf, 64.60.av, 89.75.Da, 91.30.Dk

Submitted to: *Journal of Physics: Condensed Matter*

1. Introduction

In recent years there has been an increasing interest in the study of systems that respond intermittently in the form of crackling noise when driven by an external field [1]. Examples include a variety of physical phenomena among which magnetization processes [2], plastic deformation in solids [3, 4], materials failure [5, 6] or Earth seismicity are worth mentioning [1]. Crackling noise consists of a discrete sequence of events which usually occur in the form of avalanches. Often these avalanches show absence of characteristic scales which reveals the existence of a certain kind of criticality which is usually displayed by the power law distribution of the energies or amplitudes of the avalanches. Except for earthquakes (that have strong implications for our wellbeing), little attention is paid to the study of the time scales over which avalanches occur. Probably this is due to the fact that the existence of time correlations between avalanches is not a necessary condition for avalanche criticality to occur. In fact, it is known that a temporal sequence of independent events may have energies power law distributed as has been shown for the zero-temperature Random Field Ising model with metastable dynamics [7, 8]. In any case, the existence of correlations provides a higher degree of complexity to the process and its analysis is expected to supply relevant information for a better understanding crackling noise phenomena. This is indeed the case of Earth seismicity where the study of waiting times and time correlations between earthquakes has been a subject of interest from the beginning of this research.

Martensitic transitions are another example of process that have been suggested to display avalanche criticality [9]. In these transitions avalanches are usually detected from the measurement of the acoustic emission (AE) which originates from displacement discontinuities across propagating interfaces [10]. This sound, typically recorded in the ultrasonic frequency range, carries the whole temporal and spacial information which characterizes the evolution of the internal strain field during the transformation process. Therefore, upon cooling (forward transition) or heating (reverse transition), martensitic systems evolve by relaxing from one metastable state to another within an energy landscape that characterizes the complex multiphase phase coexisting region [11]. It is worth pointing out that not only the statistical distribution of the energy of avalanches can be obtained from AE measurements but also the waiting times between avalanches.

Beside AE, other more macroscopic measurement techniques such as high sensitivity calorimetry, [12, 13] have been used in order to show that martensitic transitions do not proceed smoothly but instead occur discontinuously through an avalanche process. The interest of calorimetry is that despite its limited time response compared with the AE technique, it enables to characterize avalanches at a more macroscopic scale at which the heat conduction problem associated with the dissipation/absortion of latent heat during the relaxation between metastable states can be taken into account. That is, with this technique an absolute measurement of the energy released by the discontinuous changes can be undertaken as well as a quantification of the ratio of this released energy over the total latent heat. Acoustic emission, on the contrary, only allows for a relative

measurement of energies of the observed discontinuities, but it is able to resolve many more avalanches on a much finer time scales.

The comparison of the data obtained by both calorimetric and AE techniques [13], reinforces the suggestion of a critical distribution of avalanches in martensitic transitions: the energies of the avalanche events $\{E_k\}$, averaged over space and time, are distributed according to a power law $p(E) \sim E^{-\epsilon}$ with $\epsilon \simeq 2.15$ which implies that these systems evolve without characteristic energy scales. The phenomenon thus has many similarities with other complex dynamic critical systems. For instance, by comparing the behavior of martensites with results from seismology, such a power-law distribution of energies can be understood as the equivalent of the Gutenberg-Richter law [15] for the magnitude distribution of earthquakes that can be obtained when seismological data is accumulated from different time periods and different regions on the Earth crust. The comparison can also be extended to the studies of other first-order phase transitions: the distribution of amplitudes of the Barkhausen pulses in ferromagnets driven by an external field show also a lack of characteristic scales and different universality classes have been identified [2].

In this work we focus on the analysis of the correlations between the times of occurrence $\{t_k\}$ of the avalanches during a martensitic transformation. Many tools have been developed within the seismology community in order to analyse correlations between earthquakes. Here, inspired by these techniques, we will show that both measurement techniques, AE and calorimetry, reveal a non-Poissonian character of the transformation process. This implies that there exist small temporal correlations between avalanches. Keeping the comparison with seismology, we will propose a law similar to the so called Omori-law for aftershocks after a main earthquake [16]. A preliminary work [17], based on calorimetric measurements, already suggested the existence of corrections to Poisson behavior in the distribution of waiting times between avalanches, although the data were not conclusive. Here, by using simultaneously AE and calorimetric data we will argue that the correlations do exist. We shall also mention that the analysis presented here differs from and complements those based on Fourier Transformation that have been performed, for instance, for the case of Barkhausen noise in ferromagnets [2].

In section 2 we will present the details of the sample and experimental setup. In section 3 we will present results related to the avalanche rate and avalanche energies. In section 4, the existence of correlations will be evidenced by three different numerical analysis techniques: (A) a direct evaluation of the aftershock activity rate after big events (with energy above a selected threshold), (B) the use of the Bi-test [18] showing the failure of the local Poisson hypothesis and (C) the scaling analysis [19] of the distribution of waiting times $\delta_k = t_{k+1} - t_k$ between consecutive events. Finally, in section 5 we will summarize our results and conclude.

2. Experimental

The same sample has been used for the calorimetric and AE experiments. It is a polycrystal with composition $Cu_{67.64}Zn_{16.71}Al_{15.65}$ and a typical grain-size diameter of 1.36 mm. It has a parallelepipedic shape with a height of 3.89 mm and an octagonal base of 0.94 cm^2. The mass of the sample is 2.6503 g. More details about sample characterization, preparation and heat treatments can be found in Ref. [13]. It displays a martensitic transition from a cubic Fm3m ($L2_1$) high temperature phase to a monoclinic I2/m (18R) structure at low temperatures.

The calorimeter [20] consists of two fluxmeters —which are electrically placed in series while thermally in parallel— that press the sample. The fluxmeters are also thermally coupled to a large calorimetric block. The system is cooled down to ensure that the sample is in the low symmetry phase and then heated at a rate $R_{cal} = 0.011\,\mathrm{mK\,s^{-1}}$ (approximately one kelvin per day). During the heating process, the electromotive force provided by the fluxmeters —which is proportional to the heat exchanged by the sample— was recorded by a nanovoltmeter Keithley K2182 at a sampling rate of 12.5 Hz. Hereafter we will refer to these values as calorimetric data. The temperature of the calorimetric block was recorded by using a platinum resistance thermometer. Linearly interpolated temperature values were later assigned to every calorimetric data. High frequency noise in the calorimetric data was filtered out, after the experiment, by a fifth-order all-pole Butterworth filter with a normalized cutoff frequency equal to 8×10^{-2}.

If calorimetric data are plotted versus time or temperature, a series of bursts can be observed during the martensitic transformation. A typical example is shown in Fig. 1. Note that the burst occur above a continuous background that changes very smoothly with temperature. Both the burst and the background change sign when reversing the thermal driving. It has been suggested that the smooth and the burst response, also classified as jerks, can be associated to two different transformation mechanism [17]. Here we focus only on the analysis of the discontinuous burst that can be treated as avalanche phenomena. We restrict the analysis to a heating ramp.

By finding the local maxima and minima, we can evaluate all the positive bursts ΔV_k occurring at times t_k (or temperatures T_k). Quite generally, the time distances between consecutive positive bursts is much longer than their rising times. Thus we identify the bursts as signatures of avalanches and the slow decays as consequences of the response of the calorimeter and the smooth background curve. Assuming an exponential behavior of the instrumental transfer function of the calorimeter, the sharp bursts ΔV_k measured in voltage can be translated to avalanche energies E through the relation $E_k = \Delta V_k \tau / G$ where $\tau = 100\,\mathrm{s}$ is the time constant of the calorimeter and $G = 130\,\mathrm{mV\,W^{-1}}$ is the gain. The sequence of avalanche energies E_k at temperatures T_k corresponding to the signal in the upper panel are shown in Fig. 1(b). This corresponds to a small set of the full record of calorimetric avalanches studied here that consists of 1655 signals.

The AE setup consists of a PCI-2 acquisition system from Mistras Group (France), working at 2 MHz. The voltage signal from a piezoelectric transducer (R15LT) attached to the upper surface of the sample is amplified (60 dB), and filtered (100 kHz − 2 MHz). Individual AE events are defined when the voltage crosses a threshold at 24 dB at time t_k. The end of the event $(t_k + \Delta_k)$ is determined when the voltage crosses the threshold in the downward direction and remains below threshold for more than 100 μs. The integral of the square voltage during the duration Δ_k, normalized by a reference resistance provides a direct estimation of the energy E_k of the signal detected by the transducer. Signals have been recorded during a heating ramp between 220 K to 270 K at a rate $R_{AE} = 1.67\,\mathrm{mK\,s^{-1}}$. Note that the calorimetric ramp has been chosen to be much slower that the acoustic emission one in order to partially compensate for the slow response of the calorimeter.

Fig. 1(c) shows an example of the energies E_k at times t_k of the avalanches recorded by the AE setup. The full run analyzed in this work consists of 85, 460 signals. Note also that the total number of AE signals is much larger than the number of signals extracted from calorimetric data. Moreover the energies of the signals are much bigger for the calorimetric data than for the AE data. It is difficult to compare both energy magnitudes since it is not clear what fraction of the energy of an avalanche is released as acoustic waves and what fraction is released into heat. Moreover, only a tiny fraction of the radiated acoustic energy is recorded by the transducer. We speculate that most probably, only extremely big events or overlaps of many events are recorded by the calorimeter. In the next section we will show that very similar statistical results have nevertheless been obtained by both techniques. This is a robust indication of the existence of criticality: results do not depend on the observation scale.

3. Avalanche rate and energy distribution

The avalanche process is not homogeneous during the phase transition. Fig. 2 shows a comparison of the avalanche activity λ_{cal} and λ_{AE} (expressed as the number of recorded signals per kelvin) as a function of temperature, obtained by calorimetry and AE respectively. Note that the scales for both experimental techniques (left and right) differ by a factor one hundred. Note also that the variations of the rate during the transition show a profile that can be fitted by the superposition of two Gaussian functions and that the experimentally measured values of λ_{cal} and λ_{AE} span several orders of magnitude. The two curves show a similar behaviour, suggesting a reasonable proportionality. The fact that the second peak (at high temperatures), detected by AE is much smaller than the second peak detected by calorimetry, can be atributed to the high attenuation of the AE signals when the sample is partially transformed.

From the analysis of the full sequences we have also computed the distribution of energies $p(E)$ (Gutenberg-Richter-like laws). Fig. 3 shows the normalized histograms corresponding to calorimetry and AE in log-log scale. The straight line corresponds to the exponent $\epsilon = 2.15$ from Ref. [13]. This value is consistent with the present data,

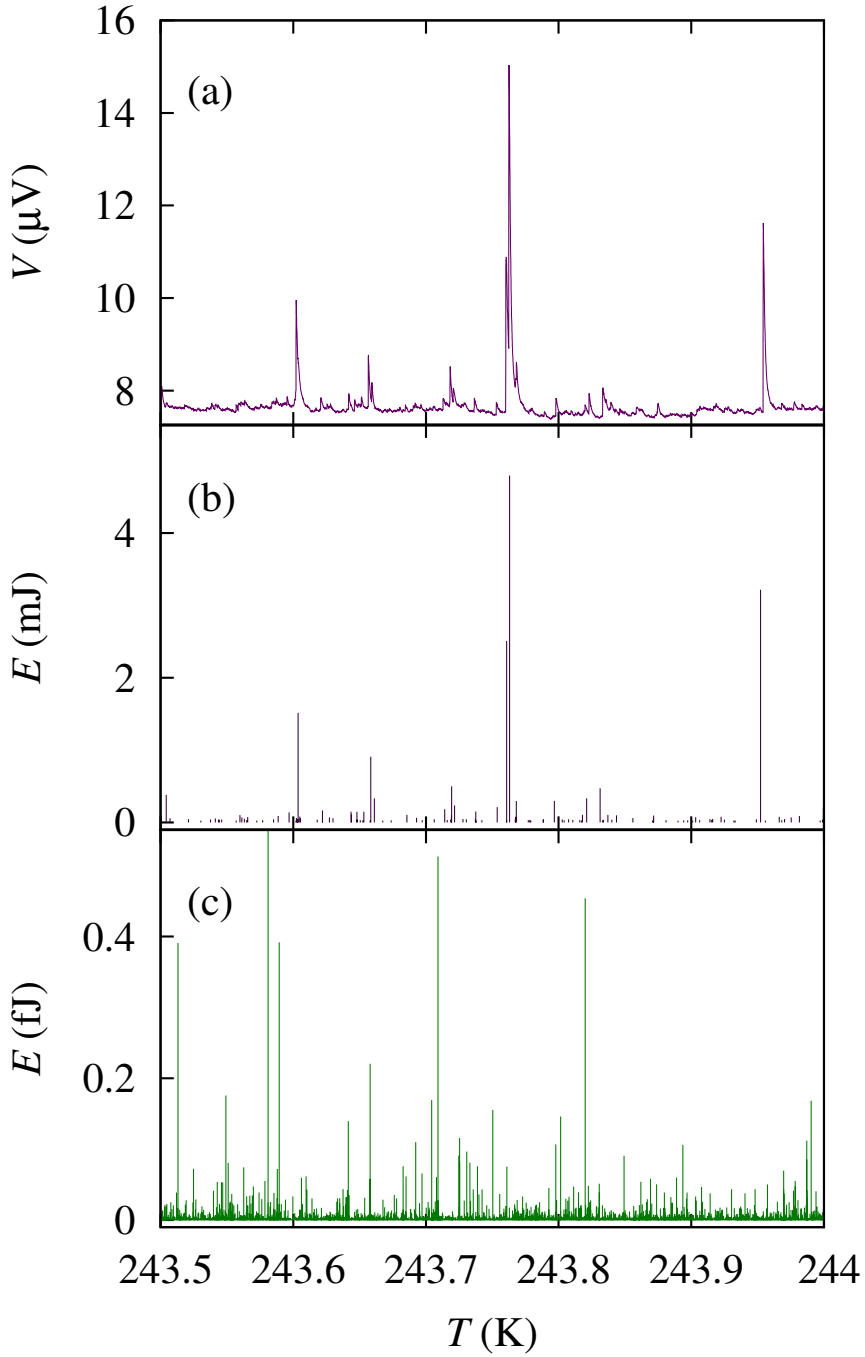

Figure 1. (a) Example of voltage signal from the calorimeter during a heating ramp (b) Corresponding sequence of calorimetric avalanches. (c) Acoustic emission avalanches. The correlation with the above sequence cannot be expected since the AE and calorimetric experiments are not performed simultaneously.

although other calorimetric experiments have found and slightly smaller exponent [17]. This exponent is not strongly universal since it is known to depend on the symmetry of the low temperature martensitic phase, the driving rate [21] and the driving mechanism

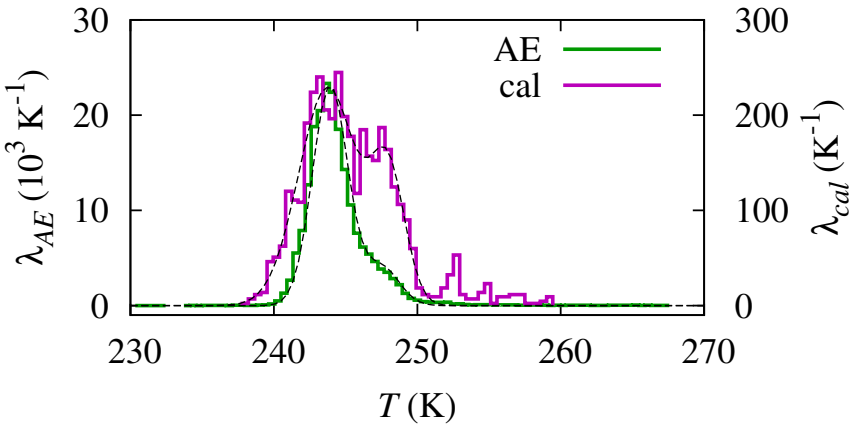

Figure 2. Activity (number of avalanches above threshold per kelvin) during the heating ramp corresponding to calorimetric avalanches (right scale) and to AE avalanches (left scale). The bins are 0.423 K for AE and 0.436 K for calorimetric data. The dashed lines show fits obtained by the sum of two Gaussian functions.

[10]. Note that there are ten orders of magnitude separating the largest AE signals from the smaller calorimetric signals. The apparent vertical offset of the two histograms is due to the fact that both are normalized independently. Both sets of energy values are hardly comparable because one corresponds to the energy recorded from the ultrasonic waves reaching the AE transducer and the other corresponds to the latent heat dissipated by the avalanches.

4. Time correlations

Beyond the non-homogeneity of the avalanche activity, which is a characteristic feature of the kinetics of martensitic phase transitions, it has been suggested that after the nucleation of a domain in the cubic phase and during its growth, local heterogeneities in the stress tensor can cause some kind of interdependence between closely recorded signals [22, 23]. A similar phenomenon, reported more than one century ago by Omori [16], is observed in seismology: the occurrence of big earthquakes, called mainshocks (MS), at time t_{MS} can trigger a sequence of aftershocks (AS) in a neighboring region with an activity rate r_{AS} that decays in time as a power-law

$$r_{AS}(t - t_{MS}) = \frac{K}{(c - t - t_{MS})^p}, \tag{1}$$

where p is an exponent close to 1 for the case of earthquakes and c and K are independent of time. Moreover, according to the so called Productivity Law [24] of aftershocks, the stronger the mainshock the more aftershocks it will trigger. Thus the numerator K is expected to depend on the the energy of the MS as $K \propto E_{MS}^{2\alpha/3}$ with the productivity exponent $\alpha \simeq 0.8$ (see Ref. [24]). This behavior has been reported in other intermittent processes [25] as well as in numerical simulations [26].

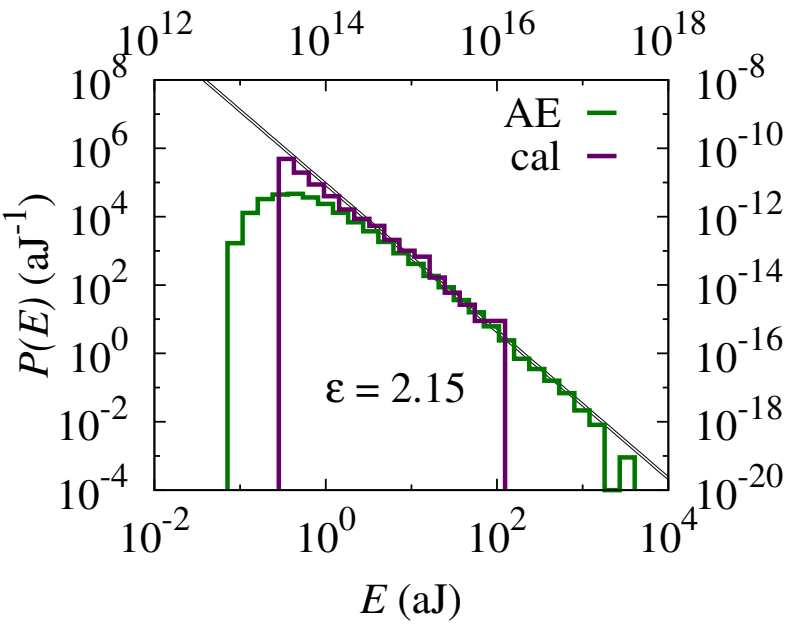

Figure 3. Energy distribution of AE and calorimetric avalanches during the full heating process. Bins are logarithmic and increase by a factor 3/2. Axes for AE (calorimetry) are left and bottom (right and top).

4.1. Aftershock sequences

The analysis of aftershock-like sequences requires a precise definition of an AS within the event series. For our calorimetric and AE data series, we adopt the same definition used within the seismology context, taking into account that we do not have access to the information of the spatial location of the events. Thus, we will consider our sample as a unique spatial region for the analysis.

Every event occurring at time t_{MS} with energy E_{MS} is considered to be a mainshock. We study the activity rate r_{AS} (number of events per time interval) as a function of the time after the MS, $\Delta t = t - t_{MS}$, until an event with energy $E > E_{MS}$ is found. This indicates the end of the aftershock sequence. Averages of the AS rates $\langle r_{AS}(\Delta t)\rangle$ are performed by considering all the sequences corresponding to MS within the windows $E_{i-1} < E_{MS} < E_i$. One then divides the time axis in (logarithmic) bins and counts the number of AS in every bin, from all sequences, and normalizes it by the number of sequences reaching that bin.

The results of this analysis are shown in Fig. 4. The legend indicates the different windows (E_{i-1}, E_i) for E_{MS}. The time $\Delta t = t - t_{MS}$ has been transformed into a temperature increase by using $\Delta T = R\Delta t$ where R is the heating rate (R_{AE} or R_{cal}). The minimum ΔT values corresponding to the aftershock sequences obtained by AE and calorimetry are separated by one order of magnitude. This is a consequence of the difference in statistics between both measurement techniques. Both AE and calorimetric data show a slight but clear decay in the production of aftershocks with an exponent

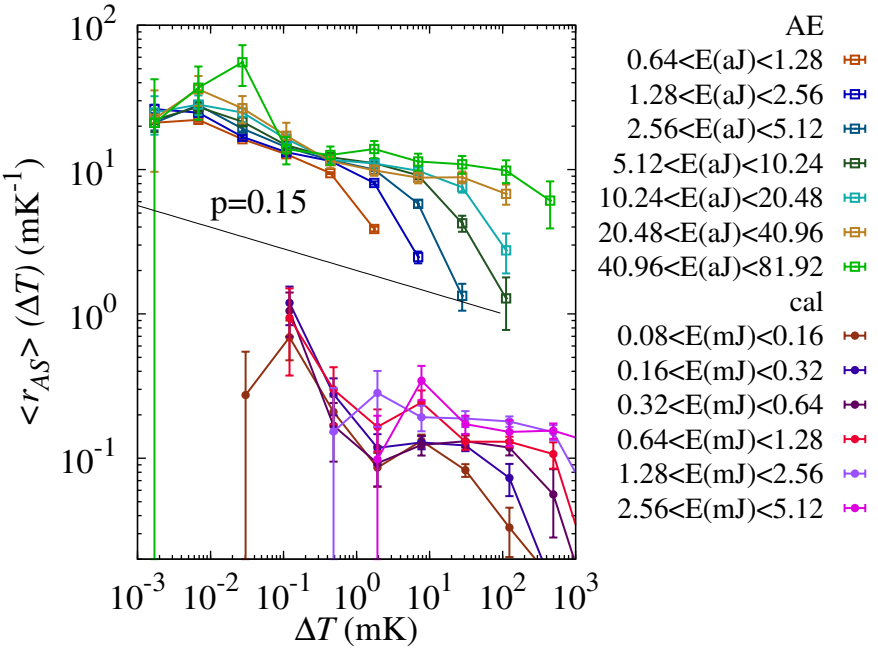

Figure 4. Comparison between the production of aftershocks in both Acoustic Emission and Calorimetry data as a function of the temperature variation after a mainshock ΔT. The straight line shows the power law behavior corresponding to an exponent $p = 0.15$. Note that if the avalanches were fully uncorrelated these plots will be flat.

$p \sim 0.15$ and a negligible dependence on E_{MS}. This may suggest a very low productivity exponent α. The immediate conclusion deduced from this result is the existence of weak correlations between avalanches. Thus, a local Poisson process is expected to be unsuitable to depict the avalanche process during the MT.

4.2. Bi-test

In order to get a more robust proof of the previous results we endeavor to show that the studied avalanche processes are non-Poissonian, even when one considers small time windows in order to correct for the non-stationary behavior. We follow Bi, Börner and Chu [18] who introduced a method to refute the null-hypothesis of local Poissonity in a point process.

Consider the sequence of events at $\{t_k\}$ depicting a point process. The Bi-test is based on the joint evaluation of the waiting time to the closest event $\delta t_k = \min\{t_k - t_{k-1}, t_{k+1} - t_k\}$ and the consecutive waiting time $\delta\tau_k$ in the same temporal direction, i.e.: $\delta\tau_k = t_{k-1} - t_{k-2}$ if $\delta t_k = t_k - t_{k-1}$ or $\delta\tau_k = t_{k+2} - t_{k+1}$ if $\delta t_k = t_{k+1} - t_k$. From the data pairs $\{\delta t_k, \delta\tau_k\}$ we can build the statistic variable

$$H_k = \frac{\delta t_k}{\delta t_k + \frac{1}{2}\delta\tau_k}, \tag{2}$$

that takes values between 0 and 1.

If data are indeed drawn from a random process which is locally Poissonian, the values δt_k and $\delta \tau_k$ will be statistically independent. The interval δt_k will be exponentially distributed according to the probability density $P(\delta t) = 2\lambda_k \exp(-2\lambda_k \delta t_k)$ and the second one $\delta \tau_k$ will be distributed according to $P(\delta \tau) = \lambda_k \exp(-\lambda_k \delta \tau_k)$ where λ_k would be the local Poissonian rate at time t_k. Consequently, doing simple algebra [18], it can be shown that the variable H_k would be uniformly distributed ($p(H) = 1$ for $0 < H < 1$), with $\langle H \rangle = 1/2$, and independent of the local Poisson rate λ_k.

Deviations from the uniform distribution indicate the existence of clustering effects. If $p(H)$ shows an excess on low and high values of H, it means that there exist big silences between groups of clustered signals. On the other hand an excess only over values close to 2/3 denotes some ordering where $\delta \tau$ is systematically smaller than $2\delta t$ (see Ref. [27]). To understand this last statement, note that if the events are drawn from an almost regularly spaced pattern we will get $\delta t_k \simeq \delta \tau_k$ and thus the variable H will distribute sharply around $\langle H \rangle = 2/3$.

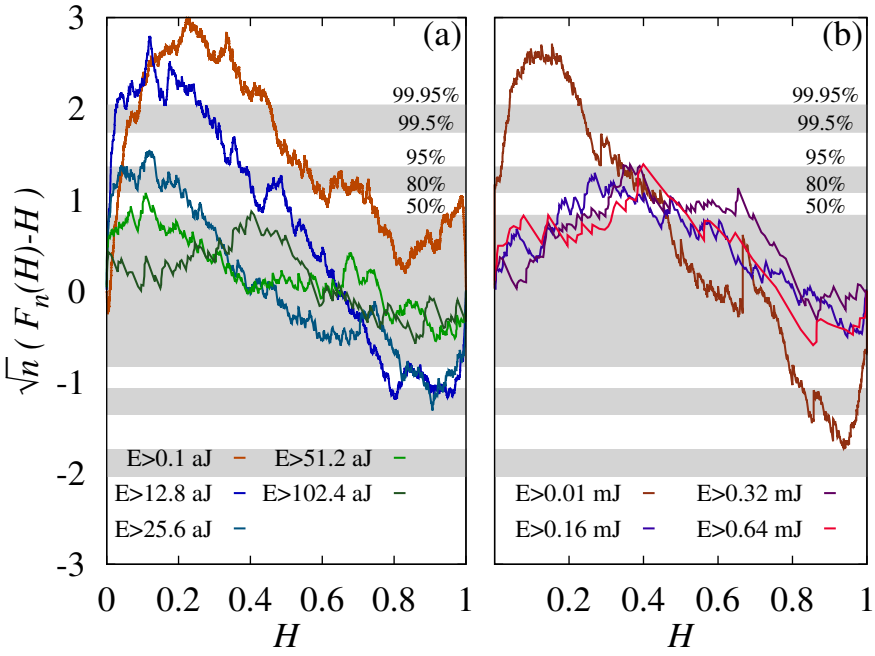

Figure 5. Kolmogorov-Smirnov test of the uniformity of the variable H obtained from the Bi-Test evaluated from the signals for AE (a) and calorimetry (b) that have energies above a certain threshold as indicated by the legend. The labels of the horizontal colored regions correspond to the p values for rejection.

Using the Bi-test, discrepancies to Poisson behavior can be quantitatively evaluated by using a Kolmogorov-Smirnov test comparing the experimental Cumulative Distribution Function $F_n(H)$ to the expected Uniform cumulative distribution function ($F(H) = H$) when the process is locally Poissonian. Fig. 5 shows the difference between both cumulative distributions normalized by the corresponding amount of data n in each sequence. The legend indicates the different energy thresholds used for the analysis.

The resulting sinusoidal shaped curves, typical in other phenomena exhibiting Omori-like production of avalanches, denote an excess of statistics in the region of high and low values of H (note the two regions with positive slope of the difference $F_n(H) - H$). The probabilities for a non-homogeneous Poisson process to exhibit such distortions from the flat behavior (the so called P-values) are very small ($P_{AE} = 2.9 \times 10^{-8}$ and $P_{cal} = 8.2 \times 10^{-7}$). Thus, we conclude in favor of the existence of some Omori-like correlations that destroy the independence of the avalanche events.

By selecting signals above increasing thresholds of energy and repeating the Bi-test analysis (see the legend in Fig. 5) we can check that, the more sparse the selected signals are, the easier is to recover a Poissonian behavior. For instance, for the AE data, using a threshold of $E > 102.4\,\mathrm{aJ}$ we get differences $F_n(H) - H$ that will clearly not allow to refute the Poisson hypothesis since they enter in the 50% confidence level region.

4.3. Waiting Times

A third test to find evidence for the existence of correlations in a point process is the analysis of the distribution of times between consecutive events, also called waiting times $\delta_k = t_{k+1} - t_k$. The study of waiting times in earthquakes over different spatial regions, with different sizes, different energy thresholds or different periods of time [19, 28, 29] revealed the collapse of the waiting time distribution $P(\delta)$ into a scaling function, when the distribution of waiting times is normalized by its mean

$$P(\delta) = \frac{1}{\langle\delta\rangle}\Phi(\delta/\langle\delta\rangle), \tag{3}$$

where the mean $\langle\delta\rangle$ depends on the studied region, on the studied period of time, on the energy threshold used for the analysis, etc., but the function Φ does not. Thus $\Phi(x)$ is referred as the Universal Scaling law and it has been checked that it describes the scaling of earthquake data and also, more recently, data obtained from the compression of porous materials [25]. Its shape displays power-law tails for the extreme values of x:

$$\Phi(x) = \begin{cases} x^{-(1-\nu)} & x \ll 1, \\ x^{-(2+\xi)} & x \gg 1. \end{cases} \tag{4}$$

Fig. 6 shows the collapse of AE data and calorimetric data by selecting different energy thresholds. Note that this analysis differs from that done previously, since there are no distinctions between mainshocks, aftershocks or foreshocks. The collapse of the curves corresponding to the two experimental techniques and for different thresholds, into a single $\Phi(x)$ curve is very good.

For a homogeneous Poisson process with a constant activity rate λ one would expect an exponential behavior $\Phi(x) = e^{-x}$ (dashed line). The effect of the non-homogeneous character of the process is to transform the exponential decay for large x to a power law decay $\Phi(x) \sim x^{-(2+\xi)}$. This decay has been explained in other contexts [25] as a consequence of how the rate $\lambda(t)$ departs or reaches 0 at the beginning and at end of

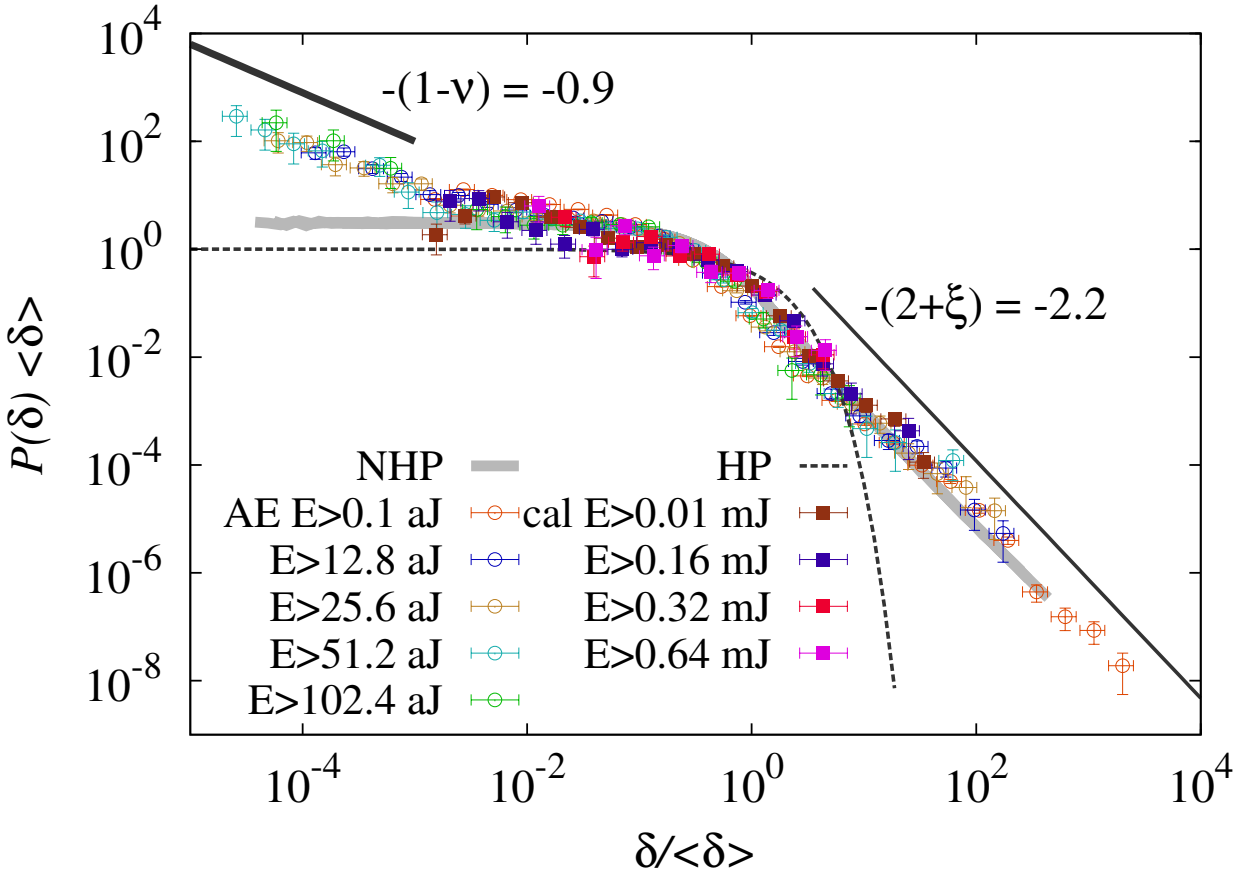

Figure 6. Collapse of the distribution of waiting times, according to the Unified Scaling Law Hypothesis. The different symbols indicate the different sets of data corresponding to AE (hollow symbols) and calorimetry (solid symbols) and different energy thresholds. The dashed line indicates the behavior expected for a homogeneous Poisson process. The thick gray continuous line indicates the expected behavior for a Non-homogeneous Poisson process with a rate λ varying according to a Gaussian function. The straight thick lines indicates the limiting exponents found for earthquake data.

the transition. We have simulated such a non-homogeneous Poisson process considering a Gaussian evolution of the rate $\lambda(t)$. We have obtained the behavior indicated by the thick gray continuous line. Simulations using a double Gaussian dependence like those fittted in Fig.2 are indistinghuishable of the thick gray line. The NHP models reproduce the observed decay of our collapsed data in the large x region with an exponent $2+\xi \sim 2.2$. The resulting value of ξ does not differ substantially from the value reported for earthquakes and compression of porous materials, $2+\xi = 2.45$ (see Refs. [[29, 25]]).

In the low δ region, the power-law behavior of the data $\Phi(x) \sim x^{-(1-\nu)}$ cannot be explained by the non-homogeneous character of the process. A possible explanation, (as has also been proposed for the case of earthquakes) is the existence of Omori-like correlations. We obtain an exponent $1-\nu$, also similar to the one obtained from

earthquakes and compression of porous materials $1 - \nu = 0.9$.

Finally, we want to note that even the data obtained with high energy thresholds that was compatible with a Poisson behavior when applying the Bi-test (see. Fig. 5), is well collapsed in the scaling presented in Fig. 6. The explanation for this apparent paradox is simply that for such small sets of data the statistics is not high enough to reveal the power-law behavior at the small x region. Strictly speaking with this third analysis technique we can see that the calorimetric data can hardly reveal the existence of the power-law behavior for low values of x.

5. Conclusions

In conclusion, we have presented clear evidences of the existence of temporal correlations within the avalanches during structural phase transitions. The results discard that the kinetics of martensitic transitions follows a Poisson process, i.e. a sequence of independent events.

Correlations have been evidenced from both Acoustic Emission and calorimetric measurements. For this last technique, since the time resolution is lower, the simple analysis of waiting times between avalanches is not enough to reveal the existence correlations. One needs the Bi-test that incorporates information of two consecutive waiting intervals to show that the process is indeed not Poissonian.

The measured correlations are similar to the Omori-like correlations in seismology, although the physical mechanism behind them can be of very different origin. We can speculate with three possible mechanisms: the most naive explanation will be that long-range elastic forces trigger the nucleation of new domains after big transformation domains occur. But other mechanisms could also be proposed. For instance we could have a coexistence of more than one physical mechanisms (propagation of needle domains and movement of wall kinks) giving rise to AE and calorimetric signals, as has recently been suggested from numerical simulations [30, 31]. A third mechanism for correlations (specialy at short waiting times) could be related to the heat propagation through the sample. This mechanism has also been discussed within seismology associated to the existence of foreshocks [32].

Acknowledgments

We acknowledge Dr. Álvaro Corral and Dr. Manuel Delgado-Restituto for fruitful discussions; and Dr. Ricardo Romero and Dr. Marcelo Stipcich for the synthesis and characterization of the sample. We acknowledge financial support from the Spanish Ministry of Economy (MAT2010-15114). EKHS thanks the Leverhulme Foundation (RG66640) and EPSRC (RG66344) for financial support. We also thank an anonymous referee for pointing us a third possible explanation for the existence of correlations associated to heat flow.

References

[1] J. P. Sethna, K.A. Dahmen, C.R. Myers, Nature **410**, 242 (2001).
[2] G.Durin and S.Zapperi in *The Science of Hysteresis* Vol II, p. 181, ed by G.Bertotti and I.D.Mayergoyz, Academic Press (2006).
[3] M. Koslowski, R. LeSar, and R. Thomson, Phys. Rev. Lett. **93**, 125502 (2004)
[4] F. F. Csikor, c. Motz, D. Weygand, M. Zaiser, and S. Zapperi, Science **318**, 251 (2007).
[5] S. Zapperi, A. Vespignani, and H. E. Stanley, Nature **388**, 658 (1997).
[6] E. K. H. Salje, D. E. Soto-Parra, A. Planes, E. Vives, M. Reinecker, and W. Schranz, Philos. Mag. Lett. **91**, 554 (2011).
[7] James P. Sethna, Karin Dahmen, Sivan Kartha, James A. Krumhansl, Bruce W. Roberts, and Joel D. Shore, Phys. Rev. Lett. **70**, 3347 (1993).
[8] M. C. Kuntz, O. Perković, K. A. Dahmen, B. W. Roberts, and J. P. Sethna, Computing in Science and Engineering **1**, 73 (1999).
[9] E. Vives, J. Ortín, Ll. Mañosa, I. Ràfols, R.Pérez-Magrané, and A.Planes, Phys. Rev. Lett. **72**, 1694 (1994).
[10] A. Planes, Ll. Mañosa and E. Vives, J. Alloys Compd (2011) doi:10.1016/j.allcom.2011.10.082
[11] K. Bhattacharya, *Microstructure of Martensite*, Oxford University Press, Oxford, U.K. (2003)
[12] A. Planes, J. L. Macqueron, M. Morin and G. Guenin, Phys. Stat. Solidi **66**, 717 (1981).
[13] M.C. Gallardo, J. Manchado, F.J. Romero, J. del Cerro, E.K.H. Salje, A. Planes and E. Vives, R. Romero and M. Stipcich, Phys. Rev. B **81** 174102 (2010).
[14] Ll. Carrillo, Ll. Mañosa, J. Ortín, A. Planes, and E.Vives Phys. Rev. Lett. **81**, 1889 (1998).
[15] T. Utsu, Pure Appl Geophys. **155**, 509 (1999).
[16] T. Utsu, Y. Ogata and R.S. Matsu'ura, J.Phy.Earth **43**, 1 (1995).
[17] F.J. Romero, J. Manchado, J.M. Martin-Olalla, M.C. Gallardo and E.K.H. Salje, Appl. Phys. Lett. **99**, 011906 (2011).
[18] H. Bi, G. Börner and Y. Chu, Astron.Astrophys. **218**, 19 (1989).
[19] P. Bak, K. Christensen, L. Danon and T. Scanlon, Phys. Rev. Lett. **88** , 178501 (2002).
[20] M. C. Gallardo, J. Jiménez, and J. del Cerro, Rev. Sci. Instrum. **66**, 5288 (1995).
[21] F. J. Pérez-Reche, B. Tadić, Ll. Mañosa, A. Planes, and E. Vives, Phys. Rev. Lett. **93** 195701 (2004).
[22] O.U. Salman, PhD dissertation, Univ. Pierre et Marie Curie, Paris, France (2009)
[23] O.U. Salman, A. Finel, R. Delville and D. Schryvers, Journ. Appl. Phys. **111**, 103517 (2012).
[24] A. Helmstetter, Phys. Rev. Lett. **91**, 058501 (2003).
[25] J. Baró, A. Corral, X. Illa, A. Planes, E.K.H. Salje, W. Schranz, D.E. Soto-Parra and E. Vives, Phys. Rev. Lett.**110**, 088702 (2013).
[26] A. Helmstetter, S. Hergarten and D. Sornette, Phys. Rev. E **70**, 046120 (2004).
[27] F. Lepreti, V. Carbone and P. Veltri, The Astronomical Journal **555**, L133 (2001).
[28] A. Corral, Phys. Rev. Lett. **92**, 108501 (2004).
[29] A. Corral, Physica(Amsterdam) **340A**, 590 (2004).
[30] E.K.H. Salje, X. Ding, Z. Zhao, T. Lookman and A. Saxena, Phys. Rev. B **83**, 104109 (2011).
[31] Z. Zhao, X. Ding, T. Lookman, J. Sun and E. K. H. Salje, Adv. Mat. **25** , 3244-8 (2013).
[32] Y.Ben-Zion, Review of Geophysics **46**, RG4006 (2008).